Applied Catalysis B: Environmental 172–173 (2015) 46–51

Contents lists available at ScienceDirect

Applied Catalysis B: Environmental

journal homepage: www.elsevier.com/locate/apcatb

Microwave-assisted synthesis of Ag-doped MOFs-like organotitanium polymer with high activity in visible-light driven photocatalytic NO oxidization

Wei Zhu [1], Peijue Liu [1], Shuning Xiao, Wenchao Wang, Dieqing Zhang *, Hexing Li *

Key Laboratory of Resource Chemistry of Ministry of Education, Shanghai Key Laboratory of Rare Earth Functional Materials, College of Life and Environmental Science, Shanghai Normal University, Shanghai 200234, PR China

ARTICLE INFO

Article history:
Received 10 January 2015
Received in revised form 2 February 2015
Accepted 8 February 2015
Available online 10 February 2015

Keywords:
Ag-doped organotitanium polymer (Ag@NH_2-MOP(Ti))
MOFs-like structure
Visible-light driven photocatalyst
NO oxidation

ABSTRACT

A novel Ag-doped MOF-like organotitanium polymer (Ag@NH_2-MOP(Ti)) was synthesized *via* a microwave-assisted coordination and polymerization reaction with 2-aminoterephthalic acid (H_2ATA) and tetra-*n*-butyl titanate ($Ti(OC_4H_9)_4$), followed by the crystal growth and assembly onto Ag nanoparticles (NPs). This Ag@NH_2-MOP(Ti) exhibited excellent activity in visible-light driven photocatalytic NO oxidization, much higher than *N*-doped TiO_2 by two times. The NH_2-MOP(Ti) absorbed visible lights to generate photoelectrons and holes, accompanied by producing $HO^•$ and O_2^- active sites for the subsequent NO oxidation into NO_3^-. The Ag NPs allowed assembly of NH_2-MOP(Ti) polymer favoring light absorbance *via* multiple reflections and also facilitated photoelectrons transfer to reduce photoelectron–hole recombination, leading to the enhanced photocatalytic activity for NO oxidation and inactivating bacteria. Moreover, it could be used repetitively owing to the high stability.

1. Introduction

Air pollution becomes crucial problem in damaging the human health and the sustainable development of both society and economy. The sweep-gas from cars, power-plants, chemical industries and plant-burning usually contains nitrogen oxides (NO_x), sulfur oxides (SO_x), carbon monoxide (CO), persistent organic pollutants (POPs) and even mercury (Hg), which were considered as the most important reason for the air pollution, which were considered as the most important reason for the air pollution, which were considered as the most important reason for the air pollution [1–3] Thus, removal NO_x is one of common targets in treating air pollution [4]. Recently, photocatalysis has received increasing attention in environmental cleaning [5–7] and the photocatalytic NO oxidization represents one of the most promising ways in removing NO_x owing to the simple operation, low cost, high efficiency, and strong durability *etc.* [8,9]. TiO_2 without or with dopants like nonmetals, metals, metal ions, and oxides are frequently employed for photocatalytic NO oxidation under UV lights irradiation [9–11], but they usually display much lower activities than thermal catalysts. Under visible-light irradiation, they exhibit extremely low activity in photocatalytic NO oxidation [8], which limits their utilization of solar lights. Recently, metal-organic frameworks (MOFs) become more and more attractive owing to their unique properties and wide applications in sensor, adsorption, catalysis, and energy storage *etc.* [12–14]. Their applications in photocatalytic dye degradation, water splitting, and CO_2 reduction have been widely reported, but most of them exhibit very poor activities [12,15–18]. No report has been found so far for the photocatalytic NO oxidation on MOFs. Herein, we reported for the first time a new Ag-loaded MOFs-like organotitanium polymer prepared by coordination and polymerization reaction between 2-aminoterephthalic acid and Tetra-*n*-butyl titanate in the presence of Ag NPs under microwave irradiation. The unique coordination bond in MOF-like network absorbed visible lights to generate photoelectrons and holes. The Ag NPs promoted the light harvesting and also facilitated photoelectron transfer to retard their recombination with holes. As a result, the as-prepared Ag@NH_2-MOP(Ti) exhibited excellent photocatalytic activity in both NO oxidization and inactivating bacteria under visible lights irradiation.

* Corresponding authors. Tel.: +86 21 64322272; fax: +86 21 64322272.
E-mail addresses: dqzhang@shnu.edu.cn (D. Zhang), hexing-li@shnu.edu.cn (H. Li).
[1] These authors contributed equally to this work.

http://dx.doi.org/10.1016/j.apcatb.2015.02.003
0926-3373/

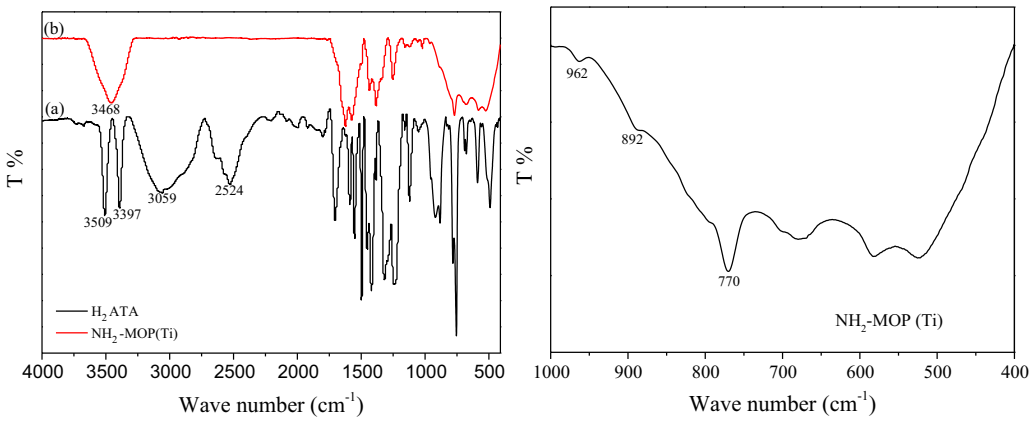

Fig. 1. FTIR spectra of (a) H_2ATA molecule and (b) NH_2-MOP(Ti) polymer. The right is the enlarged FTIR spectrum of NH2-MOP(Ti).

2. Experimental

2.1. Materials

2-aminoterephthalic acid (H_2ATA) was obtained from Sigma–Aldrich. Tetra-*n*-butyl titanate ($Ti(OC_4H_9)_4$) and Ag nanoparticles (NPs) were obtained from Aladdin. *N*,*N*-dimethylformamide (DMF), methanol (MeOH), and anhydrous ethanol (EtOH) were supplied by Sinopharm Chemical Reagent Co., Ltd. (Shanghai, China). All materials were used as received without further purification.

2.2. Sample preparation

In a typical run of synthesis, 1.1 g of H_2ATA was added into a solution containing 18 mL of DMF and 2.0 mL of EtOH and stirred at 25 °C for about 20 min to obtain a yellow solution. Then, 1.2 mL of $Ti(OC_4H_9)_4$ was added and stirred for 30 min, followed by transferring into a 40 mL quartz tube. Then, the mixture was heated to 150 °C within 5 min and kept at this temperature for 15 min controlled by a programed microwave digestion system. After being cooled down to 60 °C, the solid product was filtered, washed thoroughly with DMF and methanol, respectively. Finally, the yellow product was vacuum dried and the as-received organotitanium was denoted as NH_2-MOP(Ti). The Ag@organotitanium polymer was synthesized in the same way by adding desired amount of Ag nanoparticles in the initial stage and denoted as Ag@NH_2-MOP(Ti).

For comparison, the *N*-doped TiO_2 was also prepared under supercritical conditions [19]. Briefly, 2.5 mL of 1.0 M HNO_3 aqueous solution was mixed with 10 mL ethanol, followed by adding dropwise into a solution comprised of 40 mL ethanol and 10 mL of $Ti(OC_4H_9)_4$ at 25 °C under vigorous stirring. The formed TiO_2 gel was aged for 48 h at 40 °C and then transferred into a 500 mL autoclave containing 200 mL of ethanol and 13 of mL triethylamine (Et_3N), followed by treating under supercritical conditions at 280 °C for 2 h. After washed thoroughly with deionized water and ethanol, the obtained product was dried at 80 °C, followed by calcining at 350 °C for 8 h to remove the residual organic species.

2.3. Characterization

The morphology was observed *via* field emission scanning electron microscopy (FESEM, HITACHI S-4800) and transmission electronic micrograph (TEM, JEOL JEM-2100). UV–vis diffuse feflectance spectra (DRS) were obtained on a UV–vis spectrpphotometer (DRS, UV-2450). The Brunauer–Emmett–Teller (BET) approach was used to determine the surface area. X-ray photoelectron spectroscopy (XPS) was done on a PerkinElmer PHI 5000C ESCA system to analyze electronic states. All the binding energies were calibrated by using the contaminant carbon (C_{1S} = 284.6 eV) as a reference. The Fourier transformation infra-red spectrum (FTIR) experiments were carried out on an AVATAR 370 FT-IR spectrometer. Thermal gravimetric analysis (TGA) was performed with a PerkinElmer Pyris Diamond TG analyzer under air atmosphere with a heating ramp of 5 °C/min. The photoluminescence spectroscopy (PLS) was collected on Varian Cary-Eclipes 500 excited with 280 nm lights. The photocurrent responses in the light on–off process were determined in a homemand three electrode quartz cell containing 0.5 M Na_2SO_4 aqueous solution under visible lights (>420 nm) irradiation at an applied potential of 0.5 V vs. SCE (saturated calomel electrode) with electrochemical workstation (CHI 660D, Chen Hua Instrument Co., Ltd.).

2.4. Activity test

The photocatalytic NO oxidation was performed at an ambient temperature in a continuous flow setup equipped with an online NO–NO_2–NO_x analyzer (Thermo Scientific, Model 42i) under irradiation with two 150 W tungsten lamps equipped with a UV cut filter to cut off lights with wavelength <420 nm. The NO conversion was defined as follow:

$$\text{NO conversion}(\%) = \frac{C_0 - C}{C_0} \times 100\%$$

where C_0 is the initial balanced concentration of NO and C is the concentration of NO at a given time in photocatalytic reaction process.

The photocatalytic disinfection was carried out in a flask containing a photocatalyst and suspension of bacterial cells at 25 °C under stirring and irradiation a 300 W Xenon lamp equipped with a UV cut filter to cut off lights with wavelength <400 nm. The visible-light intensity was measured by a light meter (LI-COR, USA) and was fixed at 190 mW cm^{-2}. All glass apparatuses used in the experiments were autoclaved at 121 °C for 20 min to ensure sterility. The bacterial cells was incubated in 10% nutrient broth solution at 30 °C for 18 h. The final photocatalyst concentration and cell density were adjusted to 100 mg L^{-1} and about 1×10^7 colony forming units per milliliter (cfu mL^{-1}), respectively. Keep the reaction temperature at 25 °C and stir the reaction mixture with a magnetic stirrer throughout the experiment. Before and after the photocatalytic oxidation (PCO) treatment, an aliquot of the reaction solution was sampled at given time and immediately diluted with sterilized saline, followed by spreading onto a nutrient agar. After being incubated at 30 °C for 24 h, the number of colonies formed was counted to determine the antibacterial efficiency.

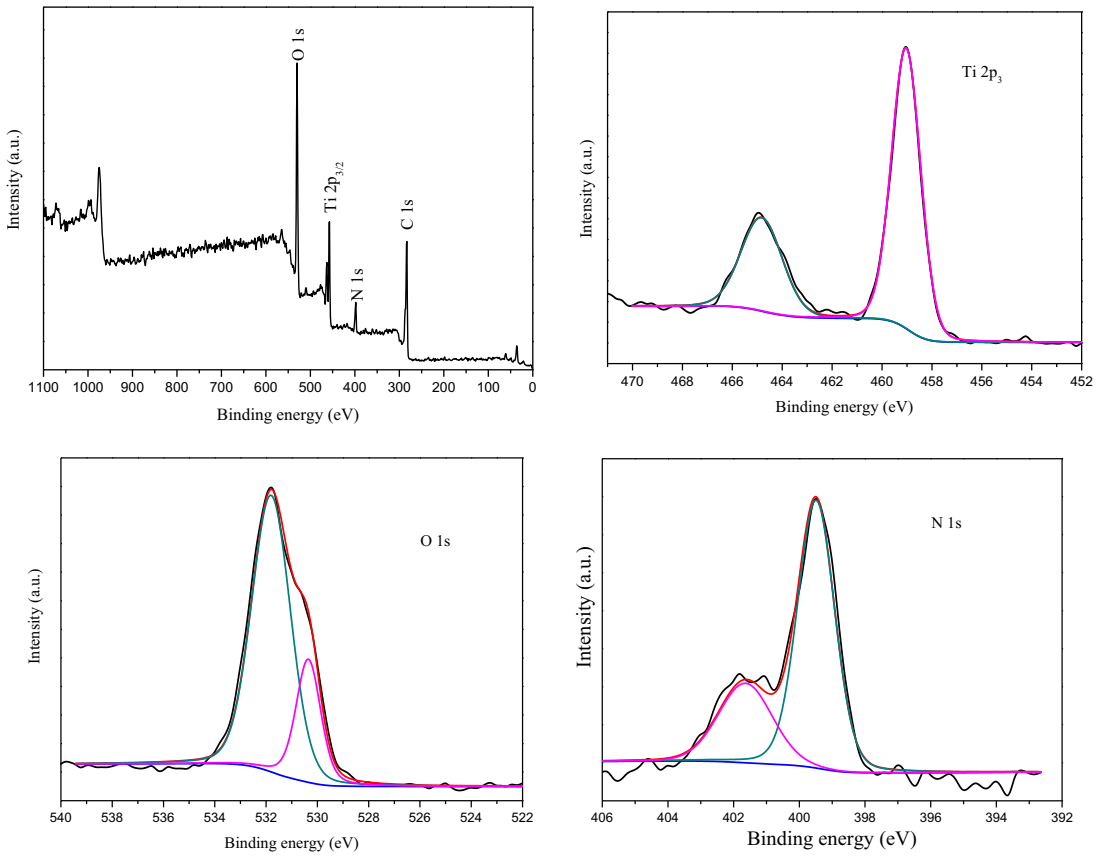

Fig. 2. XPS spectra of NH_2-MOP(Ti) polymer.

3. Results and discussion

As shown on Fig. 1, the NH_2-MOP(Ti) displayed similar FTIR spectrum to the NH_2-MIL-125(Ti) [12]. No significant vibration bands at 3059 and 2524 cm^{-1} indicative of the COOH group in the original H_2ATA molecule were observed. However, two vibration bands at 3500–3150 cm^{-1} characteristic of the —NH_2 group in H_2ATA molecule were still reserved, which were overlapped with the strong vibration band of the —OH group around 3350 cm^{-1}. Meanwhile, the special vibration peaks at 962, 892 and 770 cm^{-1} corresponding to the O—Ti—O bond were distinguished (see the enlarged spectrum on right) [20]. These results confirmed the coordination of Ti^{4+} with the —COOH group rather than the —NH_2 group in the H_2ATA molecule.

The coordination between coordination of Ti^{4+} and H_2ATA *via* —COOH groups to form NH_2-MOP(Ti) could be further confirmed by XPS spectra. As shown in Fig. 2, all the Ti species were present in +4 oxidation state, corresponding to the binding energies (BE) of 459.1 and 464.8 eV in Ti $2p_{3/2}$ and Ti $2p_{1/2}$ level, respectively. The positive BE shift in comparison with that observed in pure anatase TiO_2 [21,22], implied the coordination between Ti^{4+} and H_2ATA. This could be further confirmed by the negative BE shift of the O 1 s in NH_2-MOP(Ti) comparing to that in pure anatase TiO_2 [21,22]. The peak around BE of 531.8 eV in O 1 s level could assigned to O species in the C—O bond [23]. There were two kinds of N species. The peak around BE of 399.5 eV in N 1 s level could be attributed to N species in the NH_2 group, while the peak at about 401.5 eV could be attributed to the formation of protonated amine group in acidic medium [24].

The TGA curve in Fig. 3 demonstrated that, besides a slight weight loss from 50 to 100 °C due to the desorption of trace solvents, the NH_2-MOP(Ti) displayed a strong weight loss of about 55.6% between 160 and 500 °C, corresponding to burning removal of organic ligands to produce TiO_2 (33.3%). The mass ratio between organic ligands and TiO_2 implied that each Ti^{4+} ion coordinated with one H_2ATA in cross-linked network, leading to a porous polymer similar to NH_2-MIL-125(Ti) [12]. However, the weight of organic ligands was significantly reduced due to the unsaturated Ti^{4+} coordination, which may account for the poor crystallization degree of NH_2-MOP(Ti). As a result, the XRD pattern (Fig. S1a) showed that the NH_2-MOP(Ti) was present only in amorphous state. As show in the Fig. 4, both FESEM and TEM images revealed that the NH_2-MOP(Ti) was comprised of uniform small nanoparticles. The Ag@NH_2-MOP(Ti) remained the morphology and particle size of the original NH_2-MOP(Ti). These Ag particles with average

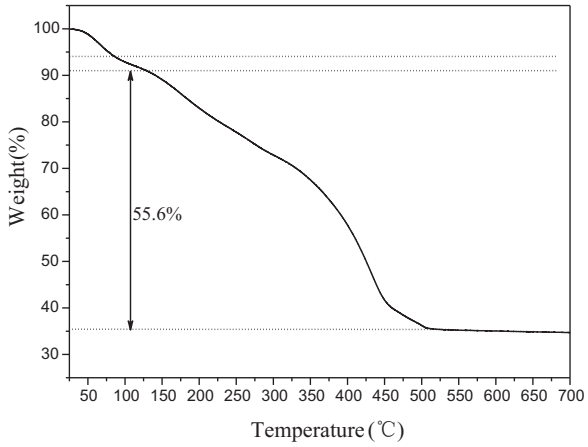

Fig. 3. Thermal analysis of NH_2-MOP(Ti) polymer under air atmosphere.

Table 1
Structural parameters of different samples.

Sample	S_{BET} ($m^2\ g^{-1}$)	V_p ($cm^2\ g^{-1}$)	D_P (nm)	D_S (nm)
NH_2-MOP(Ti)	317	0.58	7.3	19
Ag(20 mg)@NH_2-MOP(Ti)	286	0.39	5.9	22
Ag(40 mg)@NH_2-MOP(Ti)	272	0.44	6.5	23
Ag(60 mg)@NH_2-MOP(Ti)	245	0.49	6.3	24
Ag(80 mg)@NH_2-MOP(Ti)	205	0.31	6.1	29

diameter around 60–70 nm were dispersed and encapsulated by NH_2-MOP(Ti).

Based on the N_2 adsorption–desorption isotherms (Fig. S1b), they exhibited the typical IV isotherms, indicating the mesoporous structure. In addition, the BET specific surface area (S_{BET}), pore volume (V_P), pore size (D_P) and average particle diameter of different samples (D_S) were calculated. As shown in Table 1, the addition of the Ag nanoparticles caused decrease in S_{BET}, V_P and D_P, while the D_S increased. A possible reason was that microwave irradiation induced local "super hot" dots generated on the Ag surfaces, accompanied by the polymerization reaction between Ti^{4+} and H_2ATA on the Ag NPs. Thus, all the Ag nanoparticles were encapsulated by NH_2-MOP(Ti). Meanwhile, the NH_2-MOP(Ti) particle size increased owing to the rapid crystal growth induced by "super hot" dots as polymerization centers. From Fig. S2a and S2b, it could be seen that after polymerization reaction, the size of Ag NPs did not obviously change, indicating that encapsulating of NH_2-MOP(Ti) on Ag NPs could suppress the aggregation of Ag NPs under microwave irradiation. The DRS spectra in Fig. 5 demonstrated that *N*-doped TiO_2 showed spectral response in visible-light region owing to the incorporation of N into TiO_2 lattice, corresponding to the formation of intermediate energy levels [5,25]. The NH_2-MOP(Ti) also displayed strong absorbance for visible lights with the absorption edge located at 570 nm. This further confirmed the similar polymer structure to the NH_2-MIL-125(Ti), in which the COO—Ti^{4+}

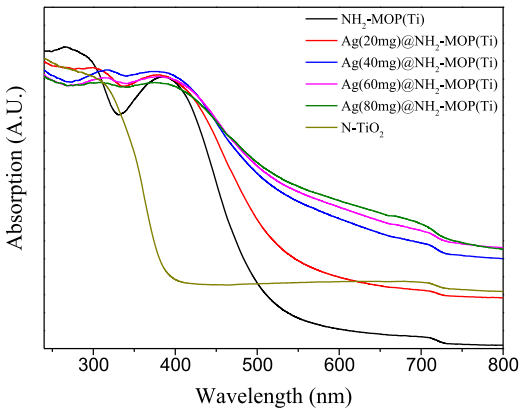

Fig. 5. UV–vis DRS spectra of different photocatalysts.

coordination bond generated the spectral response in the range from 400 to 570 nm [26]. The Ag@NH_2-MOP(Ti) displayed stronger absorbance for visible lights than that of NH_2-MOP(Ti). Obviously, the localized surface plasmon resonance (LSPR) effects from Ag NPs could be neglected due to the big size (60–70 nm). Meanwhile, the presence of Ag could enhance the dispersion (see the structural parameters in Table 1). Thus, the promoting effects could be mainly attributed to the assembly of NH_2-MOP(Ti) polymer onto Ag NPs which promoted light harvesting *via* multiple reflections. The increase of Ag amount could further enhance the visible light absorbance owing to the improved assembly of NH_2-MOP(Ti) polymer. Meanwhile, the electrochemical impedance spectroscopy (EIS) responses (Fig. S3) demonstrated the smaller semicircles of the Ag@NH_2-MOP(Ti) than that of the NH_2-MOP(Ti), indicating that decoration with Ag NPs could significantly reduce the electrochemical impedance since Ag is excellent electric conductor. Meanwhile, the photoluminescence (PL) spectra (Fig. S4) revealed

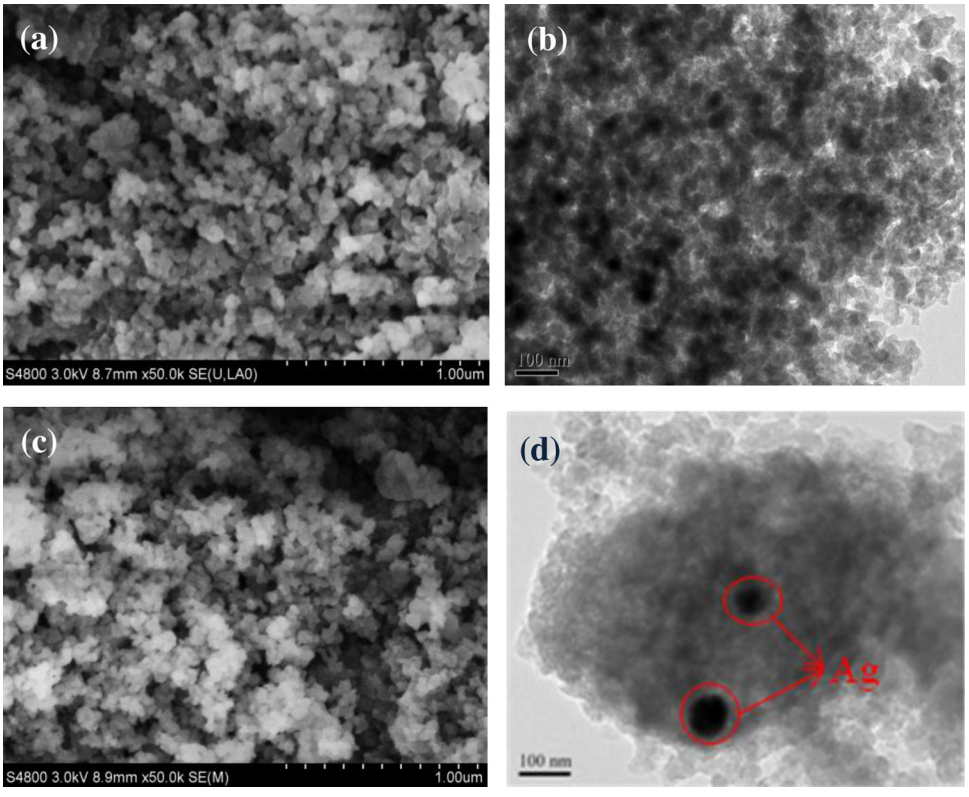

Fig. 4. The FESEM (left) and TEM (right) images of (a and b) NH2-MOP(Ti) and (c and d) Ag@NH2-MOP(Ti).

that all the Ag@NH_2-MOP(Ti) exhibited much lower peak intensity around 560 nm than the NH_2-MOP(Ti), corresponding to the lower photoelectron–hole recombination rate since the rapid transfer of photoelectrons promoted their separation from holes. As a result, the Ag@NH_2-MOP(Ti) displayed stronger photocurrent response under visible light irradiation than that of NH_2-MOP(Ti) (see Fig. S5) owing to both the enhanced light harvesting ability for generating more photocarriers and the facilitated electron-transfer for diminishing photoelectron–hole recombination rate. With the increase of Ag amount up to 40 mg, the electrochemical impedances decreased gradually owing to the enhanced electron conductivity, leading to enhanced photocurrent due to low photoelectron–hole recombination rate. However, further increase in the Ag amount resulted in an abrupt decrease in photocurrent since too many Ag nanoparticles in the NH_2-MOP(Ti) might promote the photoelectron–hole recombination. In addition, the N-TiO_2 displayed poor absorbance for visible lights due to very low content of N (<3.4% N/Ti molar ratio) incorporated into TiO_2 lattice and also showed high photoelectron–hole recombination rate due to the poor electric conductivity in the absence of Ag, which is in accordance with the result of low photocurrent.

As shown in Fig. 6 the NH_2-MOP(Ti) exhibited slightly lower activity than the typical visible-light photocatalyst (N–TiO_2) in photocatalytic Nitric oxide (NO) oxidation under visible lights irradiation. As discussed above, the NH_2-MOP(Ti) showed even higher visible lights absorbance than the N–TiO_2. Therefore, its low activity thus could be mainly attributed to the extremely poor crystallization degree, which was unfavorable for electron transfer [27], leading to the high photoelectron–hole recombination. The Ag@NH_2-MOP(Ti) exhibited much higher activity than the NH_2-MOP(Ti) owing to both the enhanced light harvesting ability and the reduced photoelectron–hole recombination rate by facilitating photoelectron-transfer. The activity gradually increased with increasing Ag content owing to the enhanced promoting effects. However, very high Ag-content was harmful for the photocatalytic activity, possibly due to the gathering of Ag NPs which might promote photoelectron–hole recombination. The Ag(40 mg)@NH_2-MOP(Ti) was thus determined as an optimum photocatalyst, which exhibited the activity almost twice as that of the N–TiO_2. Interestingly, as shown in Fig. 7, it also exhibited high activity in killing bacteria under Xenon lamp irradiation with $\lambda \geq 400$ nm, while there was no anti-bacterial activity without photocatalyst or light irradiation, indicating the excellent photocatalytic water disinfectants performance working under visible-light irradiation.

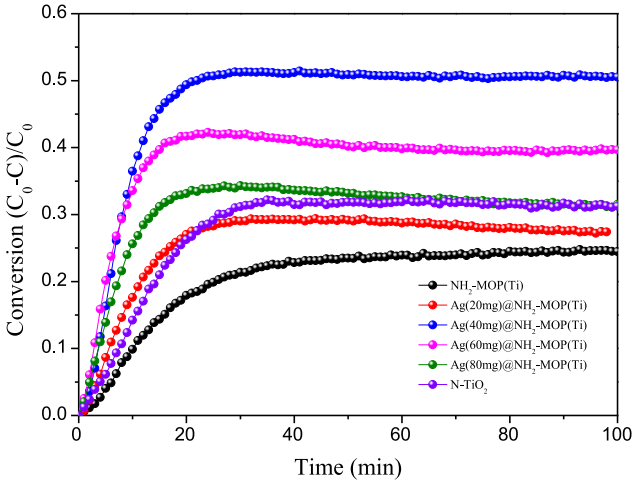

Fig. 6. Reaction profiles of photocatalytic NO oxidation under visible lights ($\lambda \geq 420$ nm) irradiation.

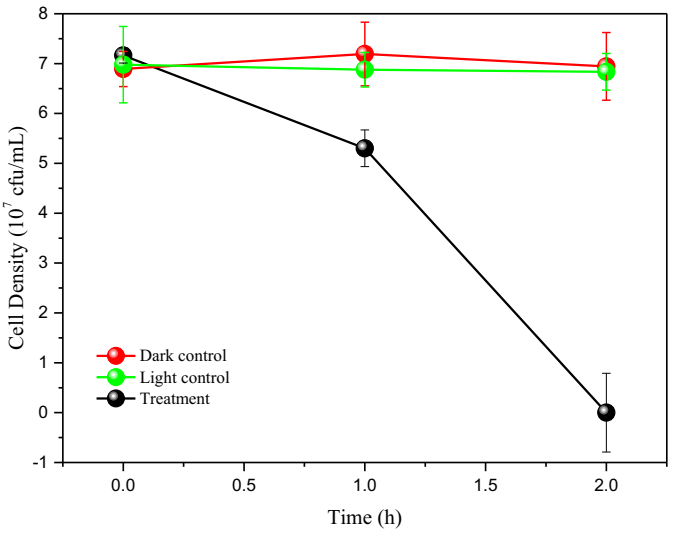

Fig. 7. Photocatalytic anti-bacteria performance of Ag(40 mg)@NH_2-MOP(Ti) for inactivating 7 log 10 bacteria, exposed to visible lights irradiation ($\lambda \geq 400$ nm) in the presence of Ag(40 mg)@NH2-MOP (Ti) (-○-); only irradiated with Xe lamp without phototacatlysts (-□-); in the presence of photocatalysts without Xe lamp irradiation (-●-).

Fig. 8 schematically illustrated the reaction mechanism for photocatalytic NO oxidation over Ag@NH_2-MOP(Ti). Similar to the NH_2-MIL-125(Ti) [28], the NH_2-MOP(Ti) polymer was formed by cross-linked Ti^{4+}–H_2ATA coordination. The visible light irradiation induced the excitation of electrons in the H_2ATA-ligand owing to the narrow energy band gap, followed by jumping from the HOMO orbital to the LUMO orbital, resulting in photoelectrons (e_{tr}^-) and holes (h_{tr}^+). Besides the recombination with the h_{tr}^+, other e_{tr}^- would transfer from the H_2ATA-ligand to Ti^{4+}, which could directly reduce Ti^{4+} into Ti^{3+} or transfer onto Ag NPs, which may retard their recombination with h_{tr}^+. Both the e_{tr}^- on the Ag NPs or the Ti^{3+} could reduce to O_2 to $O_2^{\bullet -}$ [29]. Taking into account of the molecular orbital structure $((\sigma_{1s})^2\ (\sigma_{1s}^*)^2\ (\sigma_{2s})^2\ (\sigma_{2s}^*)^2\ (\sigma_{2p})^2\ (\pi_{2p})^4\ (\pi_{2p}^*)^1)$, a single electron occupied the π antibonding orbital in NO molecule which was unstable and could be easily lost. Thus, the h_{tr}^+ on the HOMO orbital of the H_2ATA-ligand could easily capture such a single electron on the π antibonding orbital in NO molecule to form NO^+ [30,31]. Other h_{tr}^+ might directly oxidize H_2O to form the HO• radical or recombine with the e_{tr}^-. The HO• radicals also served as active sites. According to the online NO–NO_2–NO_x analysis, the $O_2^{\bullet -}$ and the HO• radicals further oxidized NO^+ into NO_3^-,

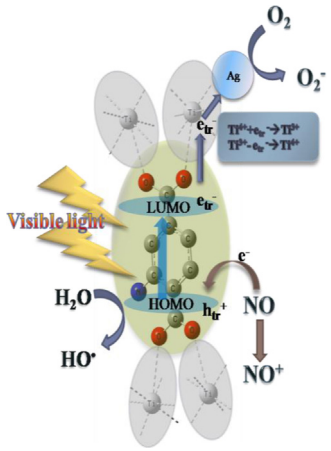

Fig. 8. Schematic illustration of mechanism for visible lights driven photocatalytic NO oxidation over Ag@NH2-MOP(Ti).

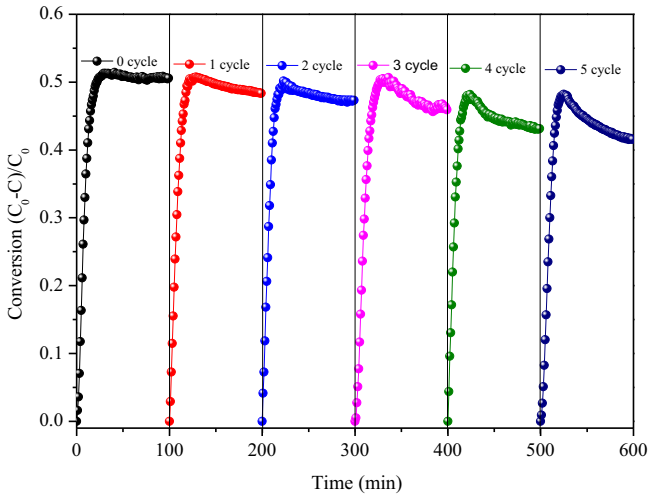

Fig. 9. Recycling test of Ag@NH_2-MOP(Ti) for photocatalytic NO oxidation under visible lights ($\lambda \geq 420$ nm) irradiation.

together with the formation of NO_2^- and as side products (see the following reaction equations) [29]. The important role of the HO• radicals from H_2O oxidation could be confirmed by the fact that the NO conversion increased by adding trace water moisture (see Fig. S6).

$$H_2ATA\text{-ligand} + h\nu \rightarrow e_{tr}^- + h_{tr}^+(\text{excited state})$$

$$e_{tr}^- + h_{tr}^+ \rightarrow \Delta(\text{ground state})$$

$$NO - e \rightarrow NO^+ \text{ and } e + h_{tr}^+ \rightarrow \Delta$$

$$h_{tr}^+ + H_2O \rightarrow HO^\bullet$$

$$e_{tr}^- \rightarrow e_{tr}^-(Ag) \text{ and } e_{tr}^-(Ag) + O_2 \rightarrow O_2^{\bullet -}$$

$$e_{tr}^- + Ti^{4+} \rightarrow Ti^{3+} \text{and } Ti^{3+} + O_2 \rightarrow O_2^{\bullet -} + Ti^{4+}$$

$$NO^+ + O_2^{\bullet -} \rightarrow NO_3^-$$

$$NO^+ + HO^\bullet \rightarrow HNO_2$$

$$HNO_2 + HO^\bullet \rightarrow NO_2 + H_2O$$

$$NO_2 + HO^\bullet \rightarrow HNO_3$$

Besides the high activity, the Ag@NH_2-MOP(Ti) also showed strong durability and could be used repetitively without significant decrease in activity (see Fig. 9). As shown by the N_2 adsorption–desorption isotherms, FTIR, XRD and TEM results (Fig. S7) of the photocatalyst before and after 5 cycles, no obvious change on the physicochemical properties and morphology of the samples after the cycled reaction was observed. We conclude that the slight decrease in the activity could be mainly attributed to the adsorption of HNO_3 onto the photocatalyst, which was accordance with the previous reports [30,32].

4. Conclusions

This work developed a novel MOFs-like organotitanium polymer *via* Ti^{4+}–H_2ATA coordination in cross-linked network under microwave irradiation. The as-prepared Ag@NH_2-MOP(Ti) exhibited very high activity and strong durability in visible lights driven photocatalytic NO oxidation and inactivation of bacteria. The NH_2-MOP(Ti) was activated by visible lights to generate photoelectrons and holes, followed by producing $O_2^{\bullet -}$ and HO• active species. The Ag nanoparticles promoted light harvesting and electron transfer to reduce photoelectron–hole recombination. To further enhance photocatalytic activity and stability, highly crystallized NH_2-MOP(Ti) with well-defined MOFs structure will be designed. Such a work is being under way.

Acknowledgements

This work was supported by NSFC (21477079, 21207090, 21237003, 21261140333), PCSIRT (IRT1269), Shanghai Government (14JC1402500, 15QA1403300h), the Doctoral Program of Higher Education (20123127120009), and Shanghai Normal University (DXL122 and S30406).

Appendix A. Supplementary data

Supplementary data associated with this article can be found, in the online version, at http://dx.doi.org/10.1016/j.apcatb.2015.02.003.

References

[1] S. Roy, A. Baiker, Chem. Rev. 109 (2009) 4054–4091.
[2] X. Huang, M.M. Li, H.R. Friedli, Y. Song, D. Chang, L. Zhu, Environ. Sci. Technol. 45 (2011) 9442–9448.
[3] G. Lammel, A. Heil, I. Stemmler, A. Dvorská, J. Klánová, Environ. Sci. Technol. 47 (2013) 11616–11624.
[4] P. Granger, V.I. Parvulescu, Chem. Rev. 111 (2011) 3155–3207.
[5] J. Schneider, M. Matsuoka, M. Takeuchi, J.L. Zhang, Y. Horiuchi, M. Anpo, D.W. Bahnemann, Chem. Rev. 114 (2014) 9919–9986.
[6] M.R. Hoffmann, S.T. Martin, W. Choi, D.W. Bahnemann, Chem. Rev. 95 (1995) 69–96.
[7] H. Chen, C.E. Nanayakkara, V.H. Grassian, Chem. Rev. 112 (2012) 5919–5948.
[8] S. Yin, B. Liu, P.L. Zhang, T. Morikawa, K.-i. Yamanaka, T. Sato, J. Phys. Chem. C 112 (2008) 12425–12431.
[9] J. Lasek, Y.-H. Yu, J.C.S. Wu, J. Photochem. Photobiol. C 14 (2013) 29–52.
[10] M. Signoretto, E. Ghedini, V. Trevisan, C.L. Bianchi, M. Ongaro, G. Cruciani, Appl. Catal. B 95 (2010) 130–136.
[11] J.S. Dalton, P.A. Janes, N.G. Jones, J.A. Nicholson, K.R. Hallam, G.C. Allen, Environ. Pollut. 120 (2002) 415–422.
[12] Y.H. Fu, D.R. Sun, Y.J. Chen, R.K. Huang, Z.X. Ding, X.Z. Fu, Z.H. Li, Angew. Chem. Int. Ed. 51 (2012) 3364–3367.
[13] J.B. DeCoste, G.W. Peterson, Chem. Rev. 114 (2014) 5695–5727.
[14] A. Bétard, R.A. Fischer, Chem. Rev. 112 (2011) 1055–1083.
[15] C. Wang, Z.G. Xie, K.E. deKrafft, W.B. Lin, J. Am. Chem. Soc. 133 (2011) 13445–13454.
[16] M.C. Das, H. Xu, Z.Y. Wang, G. Srinivas, W. Zhou, Y.-F. Yue, V.N. Nesterov, G.D. Qian, B.L. Chen, Chem. Commun. 47 (2011) 11715–11717.
[17] C.G. Silva, I. Luz, F.X.L. Xamena, A. Corma, H. García, Chem. Eur. J. 16 (2010) 11133–11138.
[18] T. Toyao, M. Saito, Y. Horiuchi, K. Mochizuki, M. Iwata, H. Higashimura, M. Matsuoka, Catal. Sci. Technol. 3 (2013) 2092–2097.
[19] Y.N. Huo, Z.F. Bian, X.Y. Zhang, Y. Jin, J. Zhu, H.X. Li, J. Phy. Chem. C 112 (2008) 6546–6550.
[20] J.C.S. Wu, Y.-T. Cheng, J. Catal. 237 (2006) 393–404.
[21] S.P. Chenakin, G. Melaet, R. Szukiewicz, N. Kruse, J. Catal. 312 (2014) 1–11.
[22] J.E. Gonçalves, S.C. Castro, A.Y. Ramos, M.C.M. Alves, Y. Gushikem, J. Electron Spectrosc. 114–116 (2001) 307–311.
[23] G.X. Zhang, S.h. Sun, D.Q. Yang, J.-P. Dodelet, E. Sacher, Carbon 46 (2008) 196–205.
[24] K.P. Wang, Q. Liu, Carbohydr. Res. 386 (2014) 48–56.
[25] R. Asahi, T. Morikawa, H. Irie, T. Ohwaki, Chem. Rev. 114 (2014) 9824–9852.
[26] Y. Horiuchi, T. Toyao, M. Saito, K. Mochizuki, M. Iwata, H. Higashimura, M. Anpo, M. Matsuoka, J. Phys. Chem. C 116 (2012) 20848–20853.
[27] J.J. Wu, X.Y. Lü, L.L. Zhang, F.Q. Huang, F.F. Xu, Eur. J. Inorg. Chem. 2009 (2009) 2789–2795.
[28] J.M. Thomas, P. Roy, Soc. A Math. Phys. 468 (2012) 1884–1903.
[29] T.L. Thompson, J.T. Yates, Chem. Rev. 106 (2006) 4428–4453.
[30] D.Q. Zhang, M.C. Wen, S.S. Zhang, P.J. Liu, W. Zhu, G.S. Li, H.X. Li, Appl. Catal. B 147 (2014) 610–616.
[31] K. Hadjiivanov, H. Knozinger, Phys. Chem. Chem. Phys. 2 (2000) 2803–2806.
[32] Z.B. Wu, Z.Y. Sheng, H.Q. Wang, Y. Liu, Chemosphere 77 (2009) 264–268.